Raman phonon piezospectroscopy in GaAs: Infrared measurements

P. Wickboldt, E. Anastassakis,* R. Sauer,† and M. Cardona
Max-Planck-Institut für Festkörperforschung, Heisenbergstrasse 1, D-7000 Stuttgart 80, Federal Republic of Germany
(Received 5 August 1986; revised manuscript received 14 October 1986)

Earlier Raman piezospectroscopic measurements for GaAs, performed with visible radiation, suggest that uniaxial stresses may be as much as 30% smaller at the surface than in the bulk of the material. We present here measurements in the forward-, backward-, and 90°-scattering configurations performed with a cw Nd-YAG (YAG denotes yttrium aluminum garnet) laser to which GaAs is transparent. We confirm the above suggestion and obtain accurate values for the deformation potentials of LO and TO phonons. We also obtain the dependence of the effective charge on uniaxial strain and compare it with recent theoretical calculations. Phenomena related to plastic deformations are observed at the highest stresses attained.

I. INTRODUCTION

Since the original work of Anastassakis *et al.*,[1] the dependence of phonon frequencies on uniaxial stress has received considerable attention.[2–6] First-principles calculations of this dependence for Si (Ref. 7) and diamond (Ref. 8) have appeared very recently, while in numerous experimental studies these data have been used for characterizing lattice-mismatched (strained) superlattices.[9] Most of the existing data on the stress dependence of phonons have been obtained by means of Raman spectroscopy. The data are presented in terms of the so-called phonon deformation potentials (PDP's) which represent the slopes of the phonon frequencies for the various irreducible components of the strain.

GaAs is the only material for which such data have been obtained with both Raman[2,4] and ir spectroscopy.[10,11] For this material (which is used as a component of many superlattices) measurements have also been performed under pure hydrostatic pressure all the way up to the phase transition (18.0 GPa).[12,13] In spite of the experimental emphasis put on such studies for GaAs, its measured PDP's are affected by considerable uncertainty which appears quite clearly when one compares data obtained under uniaxial and pure hydrostatic compressions. The uniaxial data, properly combined, yield the hydrostatic PDP's (the so-called mode Grüneisen parameters) which turn out to be as much as 30% lower than those obtained for purely hydrostatic conditions in a diamond anvil cell.[2,4,10,11] This discrepancy has been attributed to stress relaxation near the surface, in the region of penetration of visible lasers (<1 μm), or far-infrared radiation (≥ 1 μm) when the stress is applied uniaxially.[4,10] As suggested in Refs. 4 and 11, measurements with a near-infrared laser frequency to which the material is transparent become necessary.

Here we present such measurements performed with a cw Nd-YAG (YAG denotes yttrium aluminum garnet) laser (1.0642 μm) whose photon energy (1.165 eV) lies well below the direct gap of GaAs (1.429 eV at room temperature). We show that the Grüneisen parameters obtained under uniaxial conditions agree much better with the hydrostatic data. Using an oblique forward-scattering configuration, we are able to obtain data for LO phonons vibrating along the stress axis (LO singlet). These data cannot be obtained from backscattering measurements to which we are limited when the material is opaque to the laser radiation. We thus confirm that previous discrepancies are due to stress relaxation near the surface. Having overcome this limitation, and being able to measure in the oblique forward-scattering configuration, we determine accurate values for all deformation potentials of the TO and LO phonons from data for stresses along [100] and [111]. In order to check the consistency, we perform also redundant measurements for [110] stress. From the LO and TO PDP's we determine the parameters M_{ij} which give the dependence of the transverse charge on strain.[14] They are shown to agree with recent theoretical estimates.[5] Finally, we discuss our observations of plastic deformations which appear in the region of highest stresses applied.

II. MEASUREMENTS

The Raman experimental setup included a cw Nd-YAG laser (Quantronix model No. 114-R, Smithtown, NY 11787, $\omega_{\text{laser}}=9396.7$ cm^{-1}) and a germanium detector, cooled to liquid nitrogen (model No. E0-817, North Coast, Santa Rosa, CA 95406). The laser beam was chopped (18 Hz). A Jarrell-Ash model No. 25-100 double monochromator, provided with 590 lines/mm grating blazed at 1000 cm^{-1}, was used to analyze the scattered radiation. The detector signal was fed into a lock-in amplifier which was interfaced through an analog-to-digital converter, to a HP-9216 computer for analyzing the data. The measured spectral resolution was 2.7 cm^{-1}. The samples were cut as parallelepipeds of dimensions $15\times1.5\times1.5$ mm^3, x-ray oriented to within $\sim2°$, and polished. The material was obtained from Wacker Chemitronics (Burghausen, FRG) and had carrier concentrations smaller than 10^{16} cm^{-3}. Four types of sample orientations were measured designated by $(x,y,z)||([100],[010],[001])$ or **a**, $(x',y'z')||([1\bar{1}0],[110],[001])$ or **b**, $(x'',y'',z'')||([11\bar{2}],[\bar{1}10],[111])$ or **c**, and $(x''',y''',z''')||([110],[001],[1\bar{1}0])$ or **d**. The stress was always applied vertically, along z, z', z'', or z''', respec-

 ©1987 The American Physical Society

tively, and the scattered light was always detected along the horizontal axes x, x', x'', or x''', respectively. The ends of the samples were glued with epoxy into brass cups which were coupled to the stressing rig. About one cm of sample was free outside of the cups. The laser beam, with a diameter of ~ 2 mm, was focused on the center of the bar.

In the backscattering configuration we worked at nearly normal incidence (external angle of incidence $\theta \leqq 20°$) with the laser beam horizontal. In the oblique forward-scattering experiment the external angle of incidence was kept $\geqq 20°$ so as to minimize polariton effects.[15] In this case, used only with configurations **b**, **c**, and **d**, the scattering plane was chosen either horizontal or vertical. In the first case the laser beam was horizontal at an external angle of incidence θ_H, leading to a horizontal scattering wave vector $\mathbf{k}$ perpendicular to the stress axis (i.e., $\mathbf{k}||y',y'',y'''$), and thus permitting the observation of the LO doublet.[4] In the second case the laser beam was oblique at an external angle of incidence θ_V, leading to a vertical scattering wave vector $\mathbf{k}$ $(-\mathbf{k}||z',z'',z''')$, thus allowing the observation of the LO singlet.[16] To avoid problems of backlash and irreproducibility of the monochromator drive we recorded simultaneously two lines of a Hg lamp: one at 9120.4 cm^{-1} (third order) for the TO phonon and one at 9099.3 cm^{-1} (third order) for the LO phonon. All measurements were performed at room temperature.

III. EXPERIMENTAL RESULTS

A. Stress along [111]

The highest stresses reached in configuration **c** were between 1.2 and 1.3 GPa. Usually the samples broke after being under such stresses for time intervals up to about two hours. Shortly before the breaking point, they developed gradual macroscopic damages, as evidenced by the diffused transmitted laser light viewed through an ir viewer. The few Raman spectra taken while the samples were under such extreme conditions, show rather asymmetric line shapes at frequencies which fall outside of the linear trends established up to that point. These observations indicate that the material is no longer a single crystal, but rather in a plastic state led to final fracture through a time-evolving sequence of irreversible deformations. Although such data cannot be taken into account in determining the slopes of the phonon frequencies versus stress, they are, nonetheless, very informative in establishing spectroscopically the onset and monitoring of the evolution of plastic deformations as a function of crystal orientation (see following sections) and duration of loading.

For this crystal orientation, a backscattering geometry allows the transverse singlet (T_s) phonon component to be observed with the incident and scattered beam polarization $\hat{\mathbf{e}}_L$ and $\hat{\mathbf{e}}_S$, respectively, both along [111] or $[\bar{1}10]$; also, the transverse doublet (T_d) component with $\hat{\mathbf{e}}_L||[111]$, $\hat{\mathbf{e}}_S||[\bar{1}10]$, or vice versa, and the longitudinal doublet (L_d) with $\hat{\mathbf{e}}_L||\hat{\mathbf{e}}_S||[\bar{1}10]$. In the oblique forward geometry, with a vertical scattering plane, one sees the longitudinal singlet (L_s) component for $\hat{\mathbf{e}}_L||\hat{\mathbf{e}}_S||[111]$ or $\hat{\mathbf{e}}_L||\hat{\mathbf{e}}_S||[\bar{1}10]$ and the T_d component for $\hat{\mathbf{e}}_L||\hat{\mathbf{e}}_S||[\bar{1}10]$ and $\hat{\mathbf{e}}_L||[111]$, $\hat{\mathbf{e}}_S||[\bar{1}10]$, or vice versa. One problem, however, that often developed with the backward- and oblique forward-scattering configurations was the mixing of such configurations which was produced mainly by the first reflected beam from the back and front surface, respectively, inside the material. As a result, spectra of T_d or L_d could have been affected by T_s or L_s, respectively, thus introducing systematic errors in determining the slopes. To avoid such complications, we repeated and checked all data taken in the backward and oblique forward configurations, using a 90° geometry. The latter resulted in somewhat smaller signals but was cleaner and in some instances well justified. The 90° geometry, of course, could give no information about the L_s component which can only be obtained from the (vertical) oblique forward configuration.

Figure 1 shows typical spectra obtained at 0 and 1.2 GPa along [111]. The scattering configurations are $\hat{\mathbf{e}}_L||\hat{\mathbf{e}}_S||[111]$ for L_s (oblique forward) and T_s (backward), $\hat{\mathbf{e}}_L||\hat{\mathbf{e}}_S||[\bar{1}10]$ for L_d (backward), and $\hat{\mathbf{e}}_L||[\bar{1}10]$ and $\hat{\mathbf{e}}_S||[111]$ for T_d (backward and oblique forward). Figure 2 shows detailed results of shifts versus stress for the four phonon components observed in this crystal orientation. Except for L_s, all other components were obtained in the 90° geometry with $\hat{\mathbf{e}}_L||[11\bar{2}]$, $\hat{\mathbf{e}}_S||[\bar{1}10]$ for T_d and L_d, and $\hat{\mathbf{e}}_L||\hat{\mathbf{e}}_S||[111]$ for T_s. (The phonon frequencies at $X=0$ were $\omega_{TO}=268.6\pm0.2$ and $\omega_{LO}=291.8\pm0.2$ cm^{-1}.) The points in this figure are experimental and are accurate within 0.01 to 0.05 cm^{-1} depending on the quality of the spectra. The lines are the result of linear least-squares fits to the experimental points. The slopes of these fits and corresponding errors are listed in Table I. As usual, for all tetrahedral semiconductors so far measured[2,4] the singlet frequencies increase faster than the doublet frequencies with increasing stress along [111] (note, however, that for diamond the singlet increases faster for both, [111] and [001] stress[17]). From the slopes of the lines in Fig. 2 we obtain the dimensionless deformation potentials $\tilde{K}_{44}$ and the Grüneisen parameters γ listed in Table II (superscripts or subscripts L and T are used to

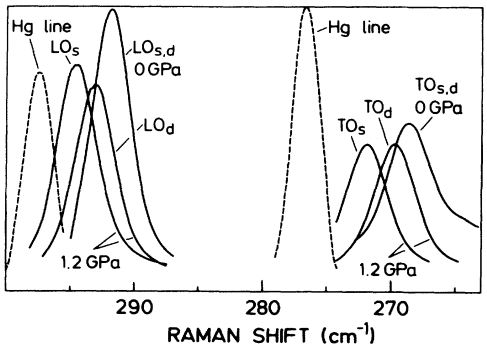

FIG. 1. Raman spectra obtained for the TO and LO phonons of GaAs at room temperature for a stress of $X=0$ GPa and for $X=1.2$ GPa along [111]. For other details, see text. The Hg calibration lines are also shown.

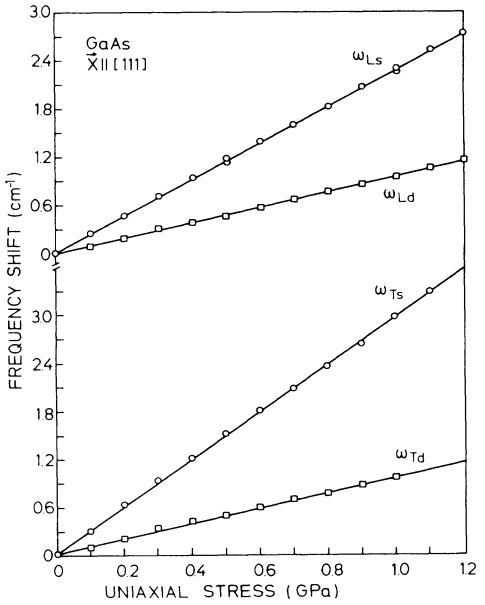

FIG. 2. Splittings and shifts measured for LO and TO phonons in GaAs under a uniaxial stress applied along [111]. These data were taken with a 90° geometry except for the L_s component which was obtained with oblique forward geometry (vertical scattering plane) from a $(11\bar{2})$ face.

identify longitudinal and transverse phonons, respectively). The equations used are

$$\tilde{K}_{44}=r\omega_0^{-2}=\frac{2(\Delta_u\omega/X)}{\omega_0 S_{44}}\ ,$$
$$\gamma=-\frac{(\Delta_H\omega/X)}{\omega_0(S_{11}+2S_{12})}\ , \tag{1}$$

where

$$\Delta_u\omega=\Delta(\omega_s-\omega_d)$$
$$\Delta_H\omega=\Delta(\omega_s+2\omega_d)/3\ .$$

and ω_0 stands for ω_{TO} or ω_{LO}, respectively.

In Eqs. (1) S_{ij} represents the elastic compliance constants. The coefficients $r=\tilde{K}_{44}\omega_0^2$ (in sec^{-2}) are sometimes used in the literature instead of $\tilde{K}_{44}$.[1,3] We take $S_{11}-S_{12}=1.54\times10^{-2}$, $S_{11}+2S_{12}=0.445\times10^{-2}$, and $S_{44}=1.68\times10^{-2}$ (in GPa^{-1}).[18] The values of $\tilde{K}^{T}_{44}$, $\tilde{K}^{L}_{44}$, γ_T, and γ_L obtained in this manner are listed in Table II and compared with other measurements. We note that earlier determinations of the parameters of the LO phonons from Raman experiments with lasers in the visible involved the use of data for γ_L obtained in separate experiments under hydrostatic pressure since the LO singlets could not be measured in backward scattering.[4]

TABLE I. Compilation of our experimental slopes of phonons in GaAs versus uniaxial stress (in cm^{-1}/GPa). Under PDP we have listed the dimensionless phonon deformation potentials which can be obtained from appropriate linear combinations of the slopes. The corresponding combinations are given under the heading $\Delta\Omega/X$. The uncertainties given for the slopes are standard deviations which correspond to the scatter of the experimental points for various repeated measurements. An uncertainty of 3% corresponding to errors in the force and the cross section must be added to them. This error has been included in Table II. θ_V and θ_H indicate oblique forward geometry in a vertical or horizontal plane, respectively. **a**, **b**, **c**, **d** refer to the three crystal orientations used in these experiments.

Crystal orientation	Scattering orientation	Polarization configuration	Phonon component	Measured slopes ($d\Omega/dX$)	PDP	($\Delta\Omega/X$)
c, **X**∥[111]	90° scattering	HH	ω_{Td}	−0.95±0.05	γ_T	$d(\omega_{Ts}+2\omega_{Td})/dX$
	90° scattering	VV	ω_{Ts}	−2.94±0.05	γ_L	$d(\omega_{Ls}+2\omega_{Ld})/dX$
	90° scattering	HH	ω_{Ld}	−0.96±0.05	$\tilde{K}^{T}_{44}$	$d(\omega_{Ts}-\omega_{Td})/dX$
	Forward θ_V	VV	ω_{Ls}	−2.25±0.05	$\tilde{K}^{L}_{44}$	$d(\omega_{Ls}-\omega_{Ld})/dX$
a, **X**∥[001]	Forward θ_V (**b**) 90° (**a**, **b**)	VH	ω_{Td}	−1.68±0.05	γ_T	
	Forward θ_H (**b**) 90° (**a**)	HH	ω_{Ts}	−1.06±0.05	γ_L	
	Forward θ_H (**b**) 90° (**a**, **b**)	VH	ω_{Ld}	−1.97±0.05	$\tilde{K}^{T}_{11}-\tilde{K}^{T}_{12}$	$d(\omega_{Ts}-\omega_{Td})/dX$
	Forward θ_V (**b**)	HH	ω_{Ls}	−0.40±0.05	$\tilde{K}^{L}_{11}-\tilde{K}^{L}_{12}$	$d(\omega_{Ls}-\omega_{Ld})/dX$
d, **X**∥[110]	Forward θ_V	VV	ω_{TdII}	−2.03±0.02		
	Backscattering			−1.84±0.02	for consistency check	
	Backscattering	VH	ω_{Ts}	−2.48±0.02		
	Forward θ_V	VH	ω_{Ls}	−2.25±0.04		
	90° scattering	HH	ω_{LdI}	−1.27±0.02		

TABLE II. Values of phonon deformation potentials (PDP's) and Grüneisen parameters compared with other Raman and ir studies. Note that in previous Raman work the PDP's of the LO phonons were not obtained directly in uniaxial stress experiments but by combining uniaxial and hydrostatic data. In the present work they are obtained solely from uniaxial data by using oblique forward-, backward-, and 90°-scattering configurations.

Crystal orientation	$\tilde{K}^{T}_{44}$	$\tilde{K}^{L}_{44}$	γ_T	$\tilde{K}^{T}_{11}-\tilde{K}^{T}_{12}$	$\tilde{K}^{L}_{11}-\tilde{K}^{L}_{12}$	γ_L	Ref.
X||[111]	−0.88±0.03	−0.53±0.03	1.35±0.03			1.07±0.03	Present
	−0.80±0.12	−0.54±0.12	0.92±0.10			0.80±0.10	4
	−0.80±0.40	−0.60±0.16	1.00±0.30			1.00±0.15	10
	−0.20±0.20						2
	−0.74±0.06	−0.48±0.06	1.15±0.06			0.89±0.05	11
X||[001]			1.23±0.03	0.30±0.03	0.70±0.03	1.11±0.03	Present
			0.78±0.10	0.24±0.14		0.66±0.10	4
			0.70±0.30	0.60±0.30	0.70±0.16	0.80±0.15	10
				0.20±0.20			2
			0.94±0.06	0.16±0.06	0.50±0.10	0.73±0.10	11
Average			1.29±0.04			1.09±0.04	Present
			0.85±0.10			0.73±0.10	4
			0.85±0.30			0.90±0.15	10
Hydrostatic			0.90±0.30				2
			1.05±0.11			0.81±0.10	11
			1.39±0.02			1.23±0.02	13

B. Stress along [001]

Here, we chose either the $(\bar{1}10)$ plane (**b** configuration) or the (100) plane (**a** configuration) as a scattering face. The L_s component is observed only from **b** in the oblique forward geometry (vertical scattering plane) with $\hat{e}_L \| \hat{e}_S \| [110]$. The remaining components (T_s, T_d, L_d) can be obtained with various scattering geometries (backward, oblique forward, or 90° scattering) from **b** or **a**, according to the usual selection rules. We applied several of them and, within error, all gave the same slopes, shown in Table I.

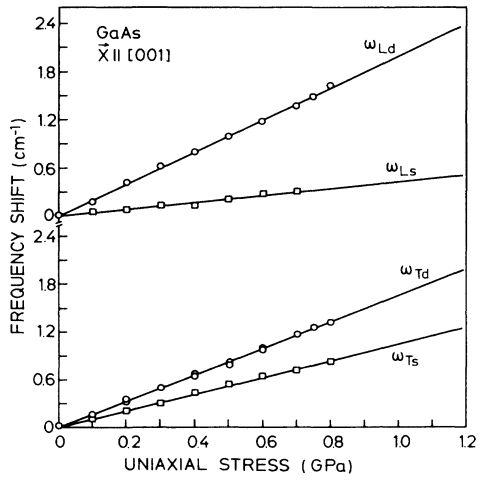

FIG. 3. Splittings and shifts measured for LO and TO phonons in GaAs under a uniaxial stress applied along [001]. The data were taken with a 90° geometry from a (100) scattering face (configuration *a*), except for the L_s component which was obtained with oblique forward geometry (vertical scattering plane) from a $(1\bar{1}0)$ face (configuration **b**).

Figure 3 shows the shift of the LO and TO phonon frequencies versus stress along [001]. The L_s component was obtained as described above while the other three components were observed with 90° geometries (Table I). The quality of data is as good as that for **X**||[111] (Fig. 2). Also, the general behavior of the crystals in the high-stress region was similar to that for **X**||[111], except that the breaking point was lower, between 0.75 and 0.85 GPa, and the time interval at which the crystals were able to sustain such high stresses were shorter, typically less than one hour. It appears therefore that the crystal enters a state of plasticity at about 0.80 GPa and is led to fracture faster than for $X=1.2$ GPa along [111]. These effects were seen rather reproducibly for many samples cut from separate boules. Thus data points above 0.80 GPa were discarded for the determination of the slopes of Table I in the [001] stress case. We note that these results correlate very well with other findings in the literature: In Ref. 19 a sudden increase in the piezoresistance for [001] stress was obtained in GaAs for X between 0.7 and 0.9 GPa. It was suggested that it might be due to plastic deformation.

The measurements for **X**||[001] also show the following peculiarity. In the low-pressure region ($0<X<0.1$ GPa) the incident beam polarized along [001] changes its polarization after crossing the sample. This effect reaches a maximum for $X\sim 0.06$ GPa. At this pressure the sample seems to be birefringent with an optical axis at $\sim 45°$ with respect to the stress direction. At higher pressures (≥ 0.1 GPa) this effect disappears and the optical axis agrees again with the stress direction. We did not find any obvious explanation of this effect which we plan to

investigate further. On account of it, however, we discarded for our linear fits any points obtained for $X < 0.1$ GPa.

We note that in Fig. 3 the doublets shift faster with X than the singlets, contrary to the results of Fig. 2. This fact is also common to all tetrahedral semiconductors but not for diamond.[17] From the slopes measured for the LO and TO frequencies versus X (Table I) and Eqs. (1), which remain valid for $\mathbf{X}||[001]$ provided one replaces $\tilde{K}_{44}$ by $\tilde{K}_{11}-\tilde{K}_{12}$, r by $p-q$, and S_{44} by $S_{11}-S_{12}$, the values of γ_T and γ_L can be obtained. The results are included in Table II.

C. Stress along [1$\bar{1}$0]

For a stress applied along [1$\bar{1}$0] the LO and TO phonons split into three components each, one polarized along the stress and two perpendicular to it. All shifts of LO and TO phonon frequencies are determined by the data of Table I, hence no new information is found. We performed, nevertheless, such measurements in order to obtain an independent check of the consistency of our results.

A straightforward calculation gives for the shift of the three components of either LO or TO phonons:

$$\begin{aligned}\Delta\omega_{dI} &= \Delta\omega_H + \tfrac{1}{6}\Delta\omega_{001} - \tfrac{1}{2}\Delta\omega_{111} ,\\ \Delta\omega_{dII} &= \Delta\omega_H - \tfrac{1}{3}\Delta\omega_{001} ,\\ \Delta\omega_s &= \Delta\omega_H + \tfrac{1}{6}\Delta\omega_{001} + \tfrac{1}{2}\Delta\omega_{111} .\end{aligned} \tag{2}$$

In Eq. (2) $\Delta\omega_s$ represents the frequency shift of the phonon vibrating along the stress, while $\Delta\omega_{dI}$ and $\Delta\omega_{dII}$ represent phonons vibrating along [110] and [001], respectively. $\Delta\omega_{001}$ and $\Delta\omega_{111}$ represent the splitting of Eq. (1) which would be obtained with stresses of the same magnitude either along [001] or along [111], respectively.

We performed Raman measurements with $\mathbf{X}||[1\bar{1}0]$ on a [110] face of a GaAs bar. With this configuration, and oblique forward-, backward-, and 90°-scattering geometries, we measured some of the components of the LO and TO phonons. The slopes from the linear fits of the data are given in Table III together with the values calculated with Eq. (2) from the data of Table I. The agreement is satisfactory, especially after one enlarges the error bars to include in each case a 3% error due to force and cross-section uncertainties. We should point out that for this stress direction plastic deformation sets in between 0.80 and 0.90 GPa, i.e., practically at the same deformation pressure as for the samples with $\mathbf{X}||[001]$.

D. Effective charge deformation potentials

In view of the reliable values of the shear splitting parameters $\tilde{K}_{44}$ and $\tilde{K}_{11}-\tilde{K}_{12}$ for the LO and TO phonons found here, it is of interest to evaluate the dimensionless tensor components $\tilde{M}_{11}-\tilde{M}_{12}$ and $\tilde{M}_{44}$ which represent the change in transverse effective charge induced by the stress.[14] We use the following equations:[4,5,14]

$$\tilde{M}_{11}-\tilde{M}_{12} = \frac{1}{2(\epsilon_0-\epsilon_\infty)}[\,\epsilon_0(\tilde{K}^{\,L}_{11}-\tilde{K}^{\,L}_{12}) - (\epsilon_\infty\tilde{K}^{\,T}_{11}-\tilde{K}^{\,T}_{12})] + \frac{k^e_{11}-k^e_{12}}{2\epsilon_\infty} , \tag{3a}$$

$$\tilde{M}_{44} = \frac{1}{2(\epsilon_0-\epsilon_\infty)}(\epsilon_0\tilde{K}^{\,L}_{44}-\epsilon_\infty\tilde{K}^{\,T}_{44}) + \frac{k^e_{44}}{2\epsilon_\infty} , \tag{3b}$$

where ϵ_∞ and ϵ_0 represent the ir and rf dielectric constants and k^e_{ij} are the photoelastic coefficients.[14] [The reader is cautioned that Eqs. (3) have been printed in Ref. 4 with a slight error, without further consequences.] Using the values of k^e_{ij}, ϵ_0, and ϵ_∞ given in Ref. 4, we find the values of $\tilde{M}_{11}-\tilde{M}_{12}$ and $\tilde{M}_{44}$ listed in Table IV. Separate values of $\tilde{M}_{11}$ and $\tilde{M}_{12}$ can be obtained from the value of the hydrostatic coefficient $\tilde{M}_{11}+2\tilde{M}_{12}$ related to γ_L and γ_T through[4,5,14]

$$\tilde{M}_{11}+2\tilde{M}_{12} = \frac{3}{\epsilon_0-\epsilon_\infty}(\epsilon_\infty\gamma_T-\epsilon_0\gamma_L) + \frac{k^e_{11}+2k^e_{12}}{2\epsilon_\infty} + \tfrac{3}{2} . \tag{4}$$

The values of $\tilde{M}_{11}+2\tilde{M}_{12}$ found with Eq. (4) from our data (with average values for γ_T and γ_L) and from the results of other studies are also listed in Table IV. The agreement between experimental and calculated values of $\tilde{M}_{11}-\tilde{M}_{12}$ and $\tilde{M}_{44}$ is very good. Our $\tilde{M}_{11}+2\tilde{M}_{12}$ also agrees within error with the hydrostatic pressure results, the difference arising from the values of γ_T and γ_L obtained in the two experiments.

TABLE III. Slopes $d\Omega/dX$ (in cm^{-1}/GPa) measured for some of the LO and TO phonons with $\mathbf{X}||[1\bar{1}0]$, compared with calculations [Eq. (2)] from the slopes given in Table I for [001] and [111] stress. The error bars of measured slopes *do not* include the 3% due to force and cross-section uncertainty. The average values used for $\Delta\omega_H$ are -1.42 ± 0.05 for LO and -1.54 ± 0.04 cm^{-1}/GPa for TO phonons.

	TO_s	TO_{dII} (average)	LO_s	LO_{dI}
Measured	-2.48 ± 0.02	$-1.93^a\pm0.02$	-2.25 ± 0.10	-1.27 ± 0.02
Calculated	-2.44 ± 0.12	-1.75 ± 0.11	-1.81 ± 0.12	-1.19 ± 0.12

[a]Average value.

TABLE IV. Values of the effective charge shear and hydrostatic deformation potentials $\tilde{M}_{11}-\tilde{M}_{12}$, $\tilde{M}_{44}$, and $\tilde{M}_{11}+2\tilde{M}_{12}$ obtained experimentally in this work compared with other values found in the literature.

	$\tilde{M}_{11}-\tilde{M}_{12}$	$\tilde{M}_{44}$	$\tilde{M}_{11}+2\tilde{M}_{12}$
Present results	1.6±0.2	1.1±0.2	3.9±1
Other data	1.5[a]	0.9[a]	1.9[a]
	1.5±0.4[b]	0.9±0.3[b]	4.9±1.9[b]
	0.9±1.3[c]	0.8±0.5[c]	3.9±2.1[c]
			2.9±0.5[d]

[a]Theory, Ref. 5.
[b]Experiment, Ref. 11, average values.
[c]Experiment, Ref. 4.
[d]From Eq. (4) using γ_T and γ_L values obtained from the hydrostatic pressure work of Refs. 12 and 13.

IV. DISCUSSION

The data presented here (Figs. 2 and 3) and the results of the calculations (Tables I–III) show clearly the advantage of performing such measurements in the region of transparency of the semiconductor. The low noise spectra and the high quality fits have allowed us to obtain the slopes of the phonon frequencies versus stress with accuracy nearly equal to that encountered in hydrostatic pressure experiments. The values of the Grüneisen parameters obtained here are much closer to the values from hydrostatic measurements, than in any previous studies. This, of course, is due to the fact that the ir laser used here probes a large portion of the cross section of the stressed material. In all previous studies of GaAs with visible lasers[2,4] or with far-ir radiation[10,11] the light probed only the near-surface regions extending from a few hundred angstroms to a few micrometers, respectively. The systematically lower values (by as much as 30%) of the Grüneisen parameters obtained in these latter studies show clearly that the hydrostatic component of the uniaxially applied stress decreases by the same amount near the surface. The stress relaxation is expected to be maximum at the surface (within 0.5 μm) and to diminish within a few micrometers from the surface. We are therefore somewhat puzzled by recent results[20] which show an *increase* in strain near the surface for Ge and Si (by as much as 30%). We believe that the discrepancy may lie in the method of applying the stress (shorter aspect ratios than in our case, contact through lead shims instead of epoxy).

It is interesting to note that our values of $\tilde{K}^{T}_{44}$ and $\tilde{K}^{L}_{44}$ obtained with $\mathbf{X}||[111]$ agree well with the most reliable sets of other measurements (Refs. 4, 10, and 11), suggesting that near the surface the hydrostatic stress probably relaxes more than the appropriate shear component. The same argument could be made also for the shear components with $\mathbf{X}||[001]$, judging from the values of $\tilde{K}^{T}_{11}-\tilde{K}^{T}_{12}$ and $\tilde{K}^{L}_{11}-\tilde{K}^{L}_{12}$. However, it is not easy to fully ascertain this fact because of the large error bars in the previous data ($\sim$50%).

The apparent differences between the present values of γ_T and γ_L and those from hydrostatic pressure work may have a technical origin. The value of $\gamma_T=1.22\pm0.03$, for instance, was obtained through a *linear* fit to the hydrostatic pressure data to 7 GPa while 1.39 ± 0.02 was obtained from a quadratic fit of data up to the phase transition (18 GPa).[12,13] It is not possible to say off hand which type of fit is more appropriate for comparison with our results, since the equation of state of GaAs deviates from the quadratic behavior in the domain up to the phase transition. Obviously, a fit of the hydrostatic data after converting pressure to volume with an analytic equation of state (e.g., Murnaghan's), and subsequent derivation with respect to the volume, would yield values of γ_T more appropriate for comparison with our low-pressure data. This was not performed since the original hydrostatic pressure data were no longer available. We can, however, state that the value γ_T obtained in this manner would lie between those found with the linear and the quadratic fits, thus leading to even better agreement with the present values.

One interesting aspect of the present work is the possibility of spectroscopically detecting the onset of plastic deformations of the crystal, as a function of such controllable parameters as crystal orientation, level of compression, and duration of loading. The observed signs of plasticity in the region of 1.2 GPa for $\mathbf{X}||[111]$ and 0.75–0.85 GPa for $\mathbf{X}||[001]$ and $[1\bar{1}0]$ are in agreement with what should be expected on grounds of plasticity theory. Indeed, the shear-stress component τ_0 which is required to produce the onset of deformations along the gliding planes (111) is the same in both cases, and is proportional to the applied stress multiplied by the corresponding Schmid factor. Since the ratio of Schmid factors in the two cases[21] is $0.27/0.41=1:1.5$ one expects that deformations (leading to fracture) will appear at compressive stresses in the ratio 1.5:1. The values observed here have exactly that ratio, i.e., 1.2:0.8. Furthermore, we find that $\tau_0=0.27\times1.2=0.32\pm0.01$ GPa for $\mathbf{X}||[111]$ and $\tau_0=0.41\times0.8=0.33\pm0.02$ GPa for $\mathbf{X}||[001]$ and $[1\bar{1}0]$. These results agree very well with the value of $\tau_0=0.31\pm0.01$ GPa inferred from the work of Lefebvre *et al.*,[22] who measured the stress-strain curve of semi-insulating GaAs deformed at room temperature under confining pressure.

We conclude this section by recognizing that Raman spectroscopy can be used as an alternative sensitive technique to monitor plastic deformations in crystals, following a variety of treatments such as, implantation, annealing, doping, hardening, etc. The results of a related study in In-hardened GaAs will be presented in a future work.

V. CONCLUSIONS

We have measured the shifts and splittings of phonons produced by uniaxial stress in GaAs using a laser to which the material is transparent. Comparison with previous data, obtained with lasers to which the material is opaque, and also with ir reflection data, confirms the conjecture that the stress is relaxed by $\sim$30% in the surface region. We have determined from our data reliable values of the tensor coefficients $\tilde{M}_{11}-\tilde{M}_{12}$ and $\tilde{M}_{44}$ which

represent the change in transverse effective charge with strain. These coefficients agree very well with recent theoretical calculations.[5] The onset of plastic deformations becomes clear from the present data and it is placed at stress levels which depend on crystal orientation, in accordance with plasticity theory.

ACKNOWLEDGMENTS

We would like to thank H. Hirt, M. Siemers, and P. Wurster for expert technical assistance and E. Kisela and his co-workers at the Max-Planck-Institut for the preparation of our samples. We would also like to thank Joachim Wagner for his major contribution in building the experimental setup and H. Alexander for information on the phenomena of plastic deformations. One of us (P.W.) gratefully acknowledges financial assistance from the Deutscher Akademischer Austauschdienst (DAAD). The work of E. A. was partially supported by the General Secretariat for Research and Technology, Greece.

---

*On leave from National Technical University, Physics Department, Zografou Campus, Athens 15773, Greece.

†Present address: AT&T Bell Laboratories, 600 Mountain Avenue, Murray Hill, NJ 07974-2070.

[1]E. Anastassakis, A. Pinczuk, E. Burstein, F. H. Pollak, and M. Cardona, Solid State Commun. **8**, 133 (1970).

[2]F. Cerdeira, C. J. Buchenauer, F. H. Pollak, and M. Cardona, Phys. Rev. B **5**, 580 (1972).

[3]E. Anastassakis, in *Dynamical Properties of Solids,* edited by G. K. Horton and A. A. Maradudin (North-Holland, Amsterdam, 1980), Vol. 4, p. 157, and references therein.

[4]A. K. Sood, E. Anastassakis, and M. Cardona, Phys. Status Solidi B **129**, 505 (1985), and references herein.

[5]E. Anastassakis and M. Cardona, Phys. Status Solidi B **129**, 505 (1985).

[6]A. D. Papadopoulos, Y. S. Raptis, and E. Anastassakis, Solid State Commun. **58**, 645 (1986); Y. S. Raptis, E. Anastassakis, M. Hünermann, and W. Richter (unpublished data for InP).

[7]O. H. Nielsen and R. M. Martin, Phys. Rev. **32**, 3792 (1985).

[8]O. H. Nielsen, Phys. Rev. B **34**, 5808 (1986).

[9]G. Abstreiter, H. Brugger, T. Wolf, H. Jorke, and H. J. Herzog, Phys. Rev. Lett. **54**, 2441 (1985).

[10]B. A. Weinstein and M. Cardona, Phys. Rev. B **5**, 3120 (1972).

[11]M. Hünermann, W. Richter, J. Saalmüller, and E. Anastassakis, Phys. Rev. B **34**, 5381 (1986).

[12]R. Trommer, E. Anastassakis, and M. Cardona, in *Light Scattering in Solids,* edited by M. Balkanski, R. C. C. Leite, and S. S. Porto (Flammarion, Paris, 1976), p. 396.

[13]R. Trommer, Ph.D. thesis, Univeristy of Stuttgart, 1977 (unpublished).

[14]E. Anastassakis, J. Phys. C **16**, 3329 (1983).

[15]C. K. N. Patel and R. E. Slusher, Phys. Rev. Lett. **22**, 282 (1969).

[16]I. Balslev, Phys. Status Solidi B **61**, 207 (1974).

[17]M. H. Grimsditch, E. Anastassakis, and M. Cardona, Phys. Rev. B **18**, 901 (1978).

[18]*Landolt-Börnstein Tables,* edited by O. Madelung, M. Schulz, and H. Weiss (Springer, New York, 1982), Vol. 17a, p. 235.

[19]D. E. Aspnes and M. Cardona, Phys. Rev. B **17**, 741 (1978).

[20]C. S. G. Cousins, L. Gerward, J. Staun Olsen, and B. J. Sheldon (unpublished).

[21]H. Alexander (private communications).

[22]A. Lefebvre, P. François, and J. di Persio, J. Phys. (Paris) Lett. **46**, 1023 (1985).